Cleanability of Mechanical Components

David Dornfeld and Sara McMains (co-PIs)
Diego Arbelaez, Miguel Avila, Adarsh Krishnamurthy,
Wei Li , and Yusuke Yasui (co-authors)
University of California, Berkeley

Abstract: We developed computer-aided planning tools for waterjet cleaning processes incorporating experimental results. We designed experiments to determine the influence of key waterjet parameters on cleaning effect and devised a computer-aided visualization and optimization scheme incorporating these parameters. In addition, we developed a particle dynamics model to simulate local waterjet interaction with target surfaces. Finally, we developed a model to predict water traps inside the workpieces based on layered volume segmentation. Our tools will aid designers and process planners in achieving efficient cleaning of geometrically complex workpieces in high-volume manufacturing.

1. Introduction: In the past few years cleanability of mechanical components became a new engineering constraint in the automotive and aerospace industry due to a rapid increase in the complexity of engines, transmissions, suspension components, etc. [1, 2]. Cleaning processes incur significant energy and consumable costs and, in many cases, cannot achieve the degree of cleanliness necessary to meet performance and service life requirements of the components. There is opportunity to increase the efficiency of cleaning processes by understanding the effect of key process parameters and developing analytical tools that predict cleaning effect at the design and process planning stages.

Among chemical, thermal, and mechanical methods for particulate contaminant removal and transport, water-based mechanical methods, where contaminant removal is driven by kinetic energy of a cleaning fluid, prove the most practical with regard to minimal damage of the substrates, energy consumption, environmental impact, and accomplishing deburring and cleaning in a single process. In particular, we focus our investigation on high-pressure waterjet cleaning for contaminant removal.

1.1. Cleaning with High Pressure Water Jets: Several studies in the literature dealt with the effect of waterjet cutting parameters on cutting performance [e.g. 3, 4, 5]. In cutting applications it is desired to create a kerf on the substrate with a given set of requirements such as dimensional accuracy, maximum depth of cut, and cutting rate. In cleaning applications, however, material removal from the substrate and surface structure damage must be minimized while ensuring removal of the desired amount of contaminants. As a result, waterjet outflow is not confined to a kerf and the impact and jet outflow characteristics differ from cutting. A threshold energy from jet impact and outflow must be surpassed to remove contaminants while avoiding undue erosion of the substrate. For the sake of cleaning process efficiency, additionally, it is necessary to spread this energy over the largest target surface area in the shortest time possible.

Relatively few authors investigated geometric and kinematic cleaning parameters. Meng, Leu and Gensky et al. [6, 7] studied the effect of static pressure, traversal speed along a straight path, and standoff distance on cleaning effect using paint coated metal as the model target material. They quantified cleaning effect in terms of the width of coating removed from the substrate. This approach only provides binary values of *local* cleaning effect and may not capture jet interaction with rough surfaces like castings and particulate contaminants on the surfaces. Erdmann-Jesnitzer [3,8] and Vijay et al. [9,10] used interrupted and ultrasonic pulsed waterjets to evaluate cyclic loading characteristics on substrate erosion and coating removal, respectively. Both showed that transient loading parameters including frequency and number of cycles can drastically affect material removal. Yet the increase in material erosion caused by discontinuous jets compared to conventional jets was realized within a narrow standoff distance range that compromises their applicability in cleaning of geometrically complex

workpieces as, for example, engine cylinder head castings.

Experimental evidence shows that material erosion caused by liquid jet impact and outflow is a highly complex phenomenon that depends on more than 22 parameters including fluid properties, target material properties, and impact parameters [11]. Yet with fixed nozzle geometry and diameter, fluid, and target material properties, the cleaning effect of waterjet impingement can be more feasibly estimated from geometry and kinematics describing jet-workpiece interaction. In addition, we include the thickness of pre-existing water layers on the surfaces that may dampen the jet impact energy [12] and the static (pump) pressure at the nozzle (P_o) which sets impact speeds (v) (as proposed by Yanaida and Ohashi [13]). Our fluid drainage model (Section 5) estimates water layer formation based on geometry and kinematics.

In our study, geometric and kinematic parameters comprise nozzle diameter (d), standoff distance (x), angle of attack (α), curvature of the target surface (ρ), traverse speed of the jet (V), angular speed of rotating nozzle carrier (ω), average jet impact speed (v), number of jet impact loading cycles (N), frequency of those loadings (F), and water layer thickness (t). With the exception of v and d (which are given by pumping pressure and nozzle geometry), the above parameters are given by the path of the waterjets, cleaning cycle time, and geometry of the target workpiece.

1.2. Removal vs. Transport Cleaning Stages – **Measurement and Simulation**: Extraction of contaminants entails separation from the surfaces and subsequent transport outside of the workpiece. Removal is caused by direct impact characteristics of waterjets, or local loading, whereas transport depends on the flow of water throughout the workpiece on a global scale. To simplify the analysis without compromising accuracy, we investigate removal and transport as independent processes. In the removal realm we are concerned with measurement, visualization, and numerical analysis of the local cleaning effect generated by the jet impact and outflow regions. In that vein, in Section 2, we present two measurement techniques to quantify the influence of geometric and kinematic parameters on cleaning effect. Second, in Section 3, we discuss visualization and optimization techniques of waterjet cleaning including the parameters we measured experimentally. Then, in Section 4, we present our particle dynamics simulation method to study local material stresses upon jet impact and outflow conditions. In the transport realm, in Section 5, we focus on our discretized simulation of the flow of water through workpieces and the detection of water traps where contaminants may accumulate and drying becomes more difficult.

2. Effect of High-Pressure Waterjet Impingement on Substrates and Measurement Methods:

Because the rate of target area coverage and long-range standoff erosion potential is critical in efficient cleaning of complex geometries, as mentioned earlier, we use a rotating, continuous waterjet nozzle carrier in lieu of nozzles traversing the surfaces in a straight path. The overlap between direct impact *footprints* of rotating jets, in addition to the overlap of the outflow footprints, generates a cyclical loading on the target that we found influences material response, in agreement with findings by Vijay and Erdmann-Jesnitzer et. al.

To quantify the effect of pump pressure and kinematic parameters on cleaning, we devised two methods based on substrate response to waterjet action: the *embedded sand method* and the *patterned surface method*.

2.1. The Embedded Sand Method: We blasted samples of sand-casted Al-Si using a single-nozzle, continuous waterjet carrier with angle of attack orthogonal to the surface. The sample surfaces, each having an area of 4 cm^2 and no curvature, contained several embedded sand particles remnant from casting cores. The cleaning effect is quantified as the percentage decrease in the number of embedded sand particles from waterjet action. Since the feed of the nozzle carrier F is considerably smaller than the tangential speed V, we approximate the locus of the nozzle footprint on the surface as a circular path, as shown in Figure 2.1.
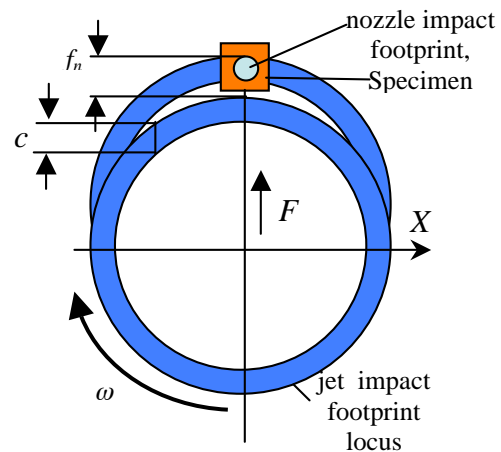
Figure 2.1. Rotating waterjet nozzle carrier parameters.

The number of jet impact loading cycles on the surface for ½ hoop blasting as a function of the distance to the centerline of the carrier, X, is given by:

$$N = \frac{c}{f_n}$$

with c defined as:

$$c = \left[\left(R + \frac{d}{2}\right)^2 - X^2\right]^{\frac{1}{2}} - \left[\left(R - \frac{d}{2}\right)^2 - X^2\right]^{\frac{1}{2}}$$
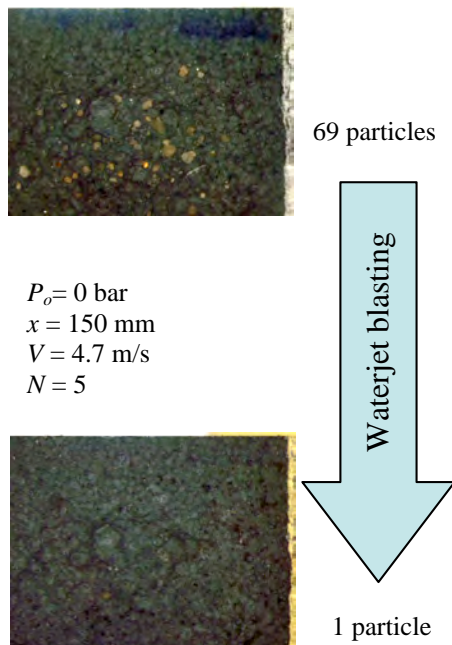
$$0 \le x \le (R - \frac{d}{2})$$

$$c = \left[\left(R + \frac{d}{2}\right)^2 - X^2\right]^{\frac{1}{2}}$$

$$(R - \frac{d}{2}) < X \le (R + \frac{d}{2})$$

where R is the radius of the rotating nozzle carrier.

We determined the percentage of sand particles removed by waterjet action using a polarized light microscope, as illustrated in Figure 2.2. The test parameters are shown in Table 2.1.

69 particles

$P_o = 0$ bar
$x = 150$ mm
$V = 4.7$ m/s
$N = 5$

Waterjet blasting

1 particle

Figure 2.2. Sand particles removed by waterjet cleaning resolved under polarized light.

Table 2.1. Experiment design for embedded sand method

P (bar)	x (mm)	V (m/s)	N
250	50	4.7	1
350	50	4.7	1
550	50	4.7	1
550	75	4.7	1
550	100	4.7	1
550	125	4.7	1
550	150	4.7	1
550	150	4.7	2
550	150	4.7	5
550	150	2.0	1
550	150	2.0	2
550	150	2.0	5
550	150	2.0	

$d = 1.2$ mm
$R = 90.0$ mm
$X = 0.0$ mm

Our results show the embedded sand method captures the influence of pressure and standoff distance on local cleaning effect. Figures 2.3 and 2.4 show the influence of pressure and standoff distance, respectively. As expected, as pressure is increased, more particles are removed. Tripling the standoff distance resulted in approximately 5% decrease in particles removed, indicative of the long-range cleaning effect of continuous waterjets.
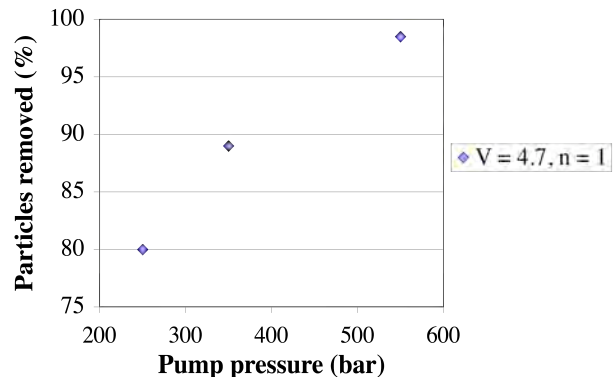
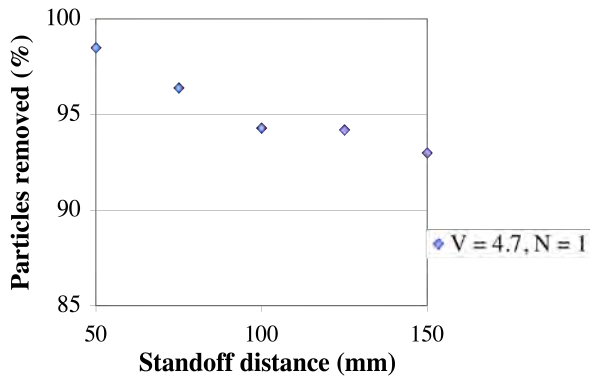**Figure 2.3.** Effect of pumping pressure on cleaning effect.

Figure 2.4. Influence of standoff on cleaning effect.

We observed that time-dependent components of the loading by waterjets, *N* and *V*, have a strong influence on cleaning effect. Figure 2.5 shows that an increase in tangential speed improves cleaning. This is explained by the higher loading frequency realized by rotating the waterjet carrier faster. Similarly, cleaning effect increases with increasing number of cycles.
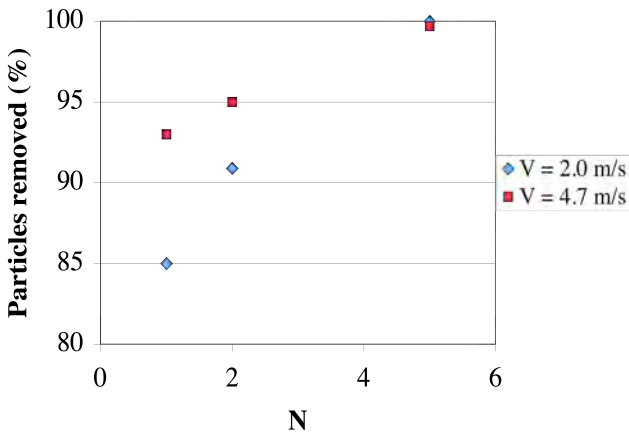

Figure 2.5. Effect of number of cycles and tangential speed on cleaning effect.

Patterned Surface Method: In order to evaluate the influence of waterjet angle of attack on cleaning effect at the impact and outflow regions, we created patterned surfaces on Al-Si samples using photolithography and chemical etching. The features are schematically shown in Figure 2.6. In this case we blasted the samples using a single, stationary waterjet with a nozzle radius of 0.6 mm and pump pressure of 550 bar. Cleaning effect is expressed as the number of features where the photoresist mask was completely eroded from the surface.
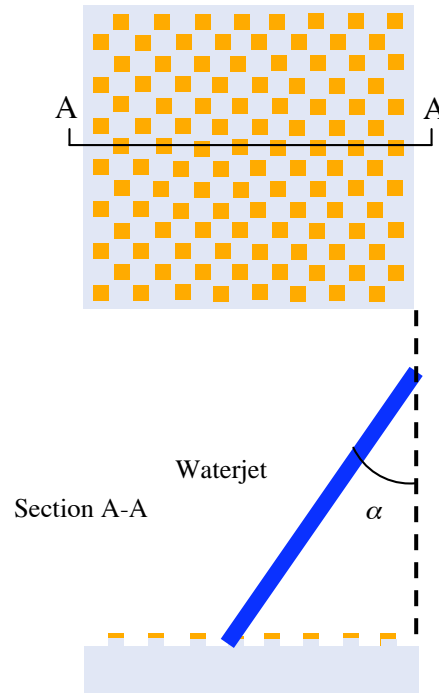

Figure 2.6. Patterned surface method for quantifying the cleaning effect of stationary waterjets
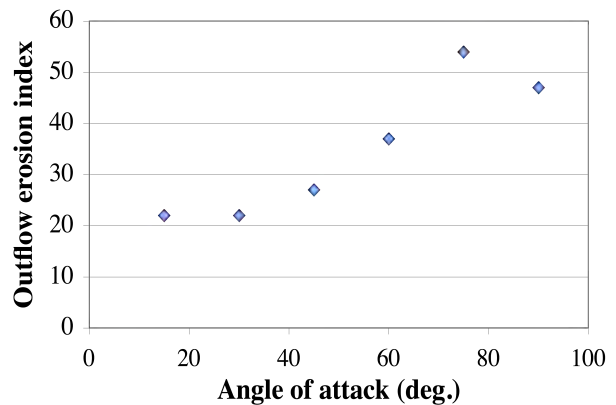

Figure 2.7. Cleaning effect of stationary waterjets as a function of angle of attack.

Results show that the outflow of jets impinging the surface at an angle from the normal direction have greater cleaning effect than approaching orthogonally and increases monotonically until a maximum inclination is reached at approximately 75° (Figure 2.7). This trend contrasts with waterjet cutting, where the degree of excavation as a function of angle of attack reaches an optimum angle of only 17° according to Rochester and Brunton [12]. Because cleaning effect isn't compromised by relatively steep angles of attack,

accessibility of interior surfaces of the workpieces with sufficient cleaning potential isn't significantly restricted by angle.

3. Visualization and Optimization of the Waterjet Cleaning Process:

As explained in the previous section, the actual cleaning process is quite complex. In order to understand the dynamic relationships that exist in an actual cleaning process, it is essential to visualize the effect of part geometry on jet-workpiece interaction. The first step required for visualizing the process is to develop a simplified model of the cleaning process. We have developed a macro scale model of the cleaning process that approximates the waterjet as a set of rays. This model can be used to understand the effect of kinematic parameters like nozzle diameter and standoff distance on cleaning. Furthermore, this model can be used to optimize these parameters. Any standard optimization technique can be used for this optimization. As a proof of concept, we used a Genetic Algorithm (GA) to optimize the process parameters for the simplified cleaning process. Analysis of the results indicates that the obtained solution is really an optimum.

3.1. Waterjet Model:

The waterjet is approximated by a set of rays as shown in Figure 3.1. The rays originate from the nozzle and have a pressure distribution that decays along the radial direction away from the center of the nozzle. The impact pressure is calculated at the points on the surface where the rays hit the surface. A model for calculating the pressure distribution of a stationary waterjet as described by Yanaida and Ohashi [13] is used for the calculations.
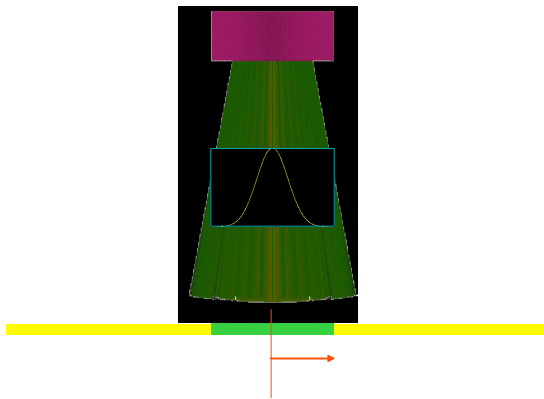
Figure 3.1. Waterjet approximated as a set of rays

The simulation program then calculates the impact pressure on the surface due to all the positions of the nozzle on a set of discrete but sufficiently dense points on the surface. Based on all these impact pressures, the cleaning efficiency is calculated.

3.2. Visualization:

To understand the influence of the geometry in the cleaning process, we have developed a visualization module. The visualization is interactive and the user can position the nozzle at different locations dynamically. The effect of cleaning is superimposed on the surface of the part using textures for easy identification of the region cleaned by the waterjet.
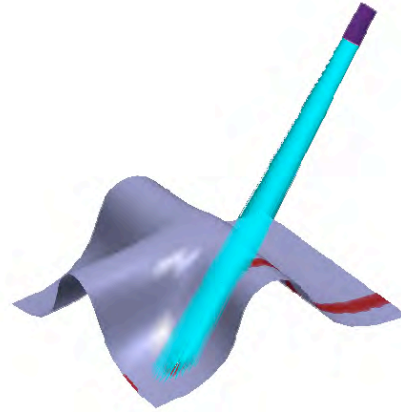
Figure 3.2. Visualization of the cleaning process.

3.3. Simplified Cleaning Process:

To make the problem tractable for the purpose of optimization, we simplified the process to reduce the design space. The simplified process involves moving a single non-rotating waterjet nozzle over a flat surface of the part to be cleaned. The nozzle is positioned at a particular standoff distance from the flat surface and is moved in a straight path.

3.4. Optimization Problem Formulation:

We formulated the optimization problem as a two-objective optimization. The first objective is to maximize the cleaning efficiency and the second objective is to minimize the time for the process. We optimized the cleaning process with respect to the design variables: standoff distance (x), angle of attack (α), and nozzle diameter (d). The optimization model also takes in some fixed parameters, including pressure (P_0), jet-spreading coefficient (C), and flow resistance factor (k).

The main constraint for the optimization is that the impact pressure should not be so high that it damages the surface of the part being cleaned. There are also some physical constraints on the maximum and minimum standoff distances and attack angles.

3.5. Genetic Algorithm:

The objective functions in this optimization problem are complex, nonlinear, and do not have an explicit expression. Therefore, a

black-box optimization technique best suited for obtaining a solution. We chose to use a GA for solving this problem because it does not require continuity or differentiability of objective functions, and can handle simple constraints. It loosely mimics biological evolution based on Darwin's theory of natural selection. The implementation used Matthew Wall's genetic algorithm library [14].

3.6. Results: Since the problem is a multi-objective optimization, it does not have a single optimal solution. The set of all solutions that are optimal is called the Pareto front and we constructed it using the ε-constraint method [15]. Figure 3.2 shows the results of the optimization along with the Pareto front in the objective domain. The scale on the *y*-axis is inverted to make it easier to read the graph, since we want *maximum* cleaning efficiency (but minimum time).
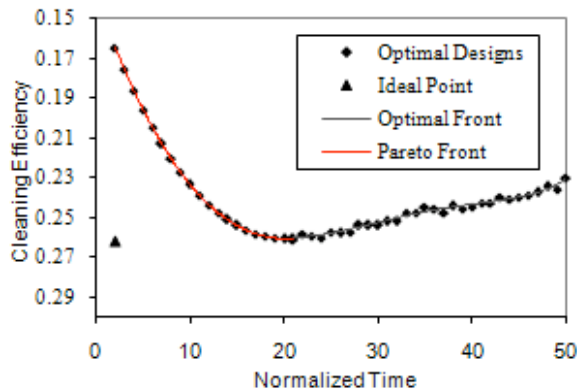
**Figure 3.3**. Results of the optimization showing the Pareto front (Note inverted scale on the *y*-axis).

There are different methods to choose a particular design from the Pareto front. We can use the ideal point (plotted at an *x*-value equal to the best time found without regard to efficiency, and a *y* value equal to the best efficiency found without regard to time) as a reference to choose an optimal design that is close to it. However, there are also several choices for defining "closeness", for example, the L^1, L^2, or L^{inf} norms. With our Pareto front, using the L^2 norm, the best design obtained has $x = 100mm$, $\alpha = 45°$, and $r_0 = 1.64mm$. These results were presented at the 2007 Workshop on Cleanability in Manufacturing [16], where we confirmed that our results agree very closely with values used in industry which were arrived at after months of experimentation.

4. Particle Dynamics Simulation of Cleaning Processes: Ideally, one would be able to simulate the entire cleaning process at a large scale on a complex part. For example, this could be done by tracking the trajectories of individual droplets to determine where they strike the surface and the cleaning effect from this droplet-surface interaction. However, this would be computationally expensive. In order to alleviate this, a multi-scale simulation can be used, where the large scale carries information such as the direction and velocity of the flow and the small scale is made of many small droplets where detailed information about the waterjet-surface interaction is determined. From the small scale, the cleaning efficiency on the surface can be determined as a function of the jet and surface parameters. The outflow condition of the jet can also be determined and used in reflections of the jet from the surface. This information from the small-scale can then be tabulated and used in the large-scale simulation, which can be described by a ray-tracing algorithm as shown in the previous section.

For the small-scale we have developed a hard particle simulation to model a waterjet striking a surface. This follows the approach taken by Zohdi [17] for granular flows. In this simulation, the position of the particles, which represent groups of droplets coming from the waterjet, is tracked over time as they come to the surface and rebound away from the surface. We do this by computing the forces on each particle and solving the equations of motion. The force interactions that we consider are particle-particle and particle-surface interactions, although the model can easily be extended to include other interactions such as the drag force from the air phase acting on the droplet. We modeled the particle-particle and particle-surface interactions through coefficients of restitution and friction. This can be tuned to best model fluid droplets. For the cleaning process it is critical to determine the cleaning efficiency on the surface in terms of possible input parameters. For example, these may include the angle of attack, the pressure, and the nozzle size and shape.

4.1. Simulation Details: Figure 4.1 shows a diagram of the simulation. Particles are first randomly placed in the inflow region. As the simulation progresses the particles that leave the inflow region are replaced by new particle at the top of the inflow box. We do this to keep the volume fraction of particles in air fixed over time. As particles leave the outflow region they are removed from the simulation. Using this simulation the following responses of the waterjet can be determined: the effect of the size of the particles on the response of the system, the steady and continuous response of the density and velocity of the flow, and the average stress on the surface.
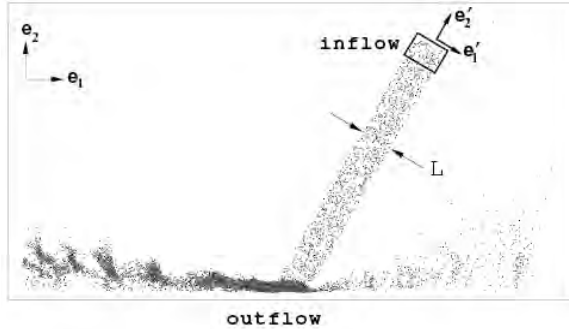
Figure 4.1. Snapshot of the local jet simulation showing the inflow and outflow regions.

4.2. Size Effects: We carried out several simulations, each time increasing the number of particles in the inflow region while decreasing their size subject to the constraint that their volume fraction was held fixed. Figure 4.2 shows how the kinetic energy of the entire system varies as the number of particles is increased. As the number of particles increases the kinetic energy increases monotonically and approaches a constant value. This implies that the waterjet can be modeled with particles that are larger than the real size of the water droplets, thus, one particle can represent many droplets. This result is critical since it allows for a computationally efficient algorithm without having to discretize down to the single droplet size scale.
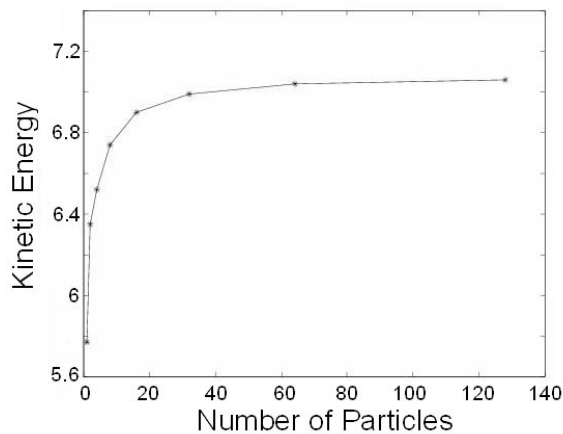
Figure 4.2. Kinetic energy of the entire system as a function of the number of particles introduced in the inflow region**.**

4.3. Continuous-Steady Response: In order to compute a "continuous" and "steady" response, we use time and volume averaging. For example Figure 4.3 shows the time and volume averaged density of the waterjet. For each instant in time, the density is computed in each of the grid cells shown in Figure 4.3. This gives the "continuous" density of the system, where in this case the density is the total mass of the droplets in the grid cell divided by the volume of the grid cell. For each instant in time the density in each grid cell is determined and is then averaged over the entire time of the simulation to determine the "steady" response. While the example in Figure 4.3 shows the density, this procedure can be carried out for any desired quantity such as the velocity or energy of the flow.
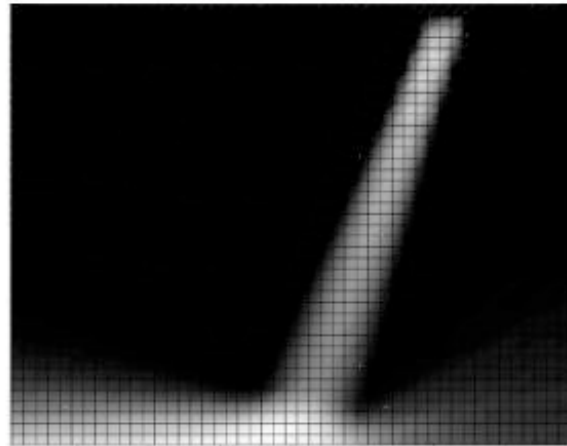

Figure 4.3. Time and volume averaged density of a waterjet striking a surface. The lighter regions represent a higher density.

4.4. Average Surface Stress: We can compute the average surface stress similarly to the "continuous" and "steady" response. However, in this case the surface (as opposed to the waterjet) is discretized into grid cells. The average stress is defined in a similar way to the pressure in kinetic theory, where the pressure is the sum of the impulses on the surface per unit time per unit area. In this case, we run the simulation for a given time, T, and the impulses are summed in each grid cell. The average surface stress in each grid cell is then given by:

$$S = \frac{\sum_i (\overline{F}\delta t)_i}{TA}$$

where $(\overline{F}\delta t)_i$ is the impulse due to particle i striking the surface, and A is the area of the grid cell. Figure 4.4 shows an example of the average stress computation, where the average tangential or shear stress is plotted as a function of the angle of attack. These simulations can be carried out for varying flow and surface parameters

and the results can be tabulated for use in a large-scale simulation.
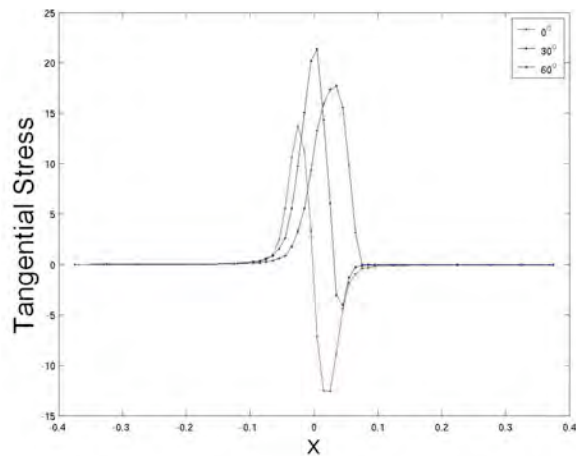
Figure 4.4. Average tangential stress profile as a function of the angle of attack.

5. Modeling Cleaning Fluid Drainage to Locate Cleaning-Incompatible Features:

In this section, we explain how we identify cleaning-incompatible features on mechanical parts. Specifically, we focus on locating recirculation zones or "dead zones" where the water from water jets is trapped, with the ultimate goal of finding configurations that minimize or avoid such local water traps.

In order to provide interactive "Design for Cleanability" (DFC) feedback to designers, we need a real-time algorithm that does not rely on computationally expensive method such as CFD simulations. We propose a new algorithm to simulate a steady-state solution of free-surface flow (purely gravity driven) using a new geometric volume segmentation method. We assume that the input is given as a polygonal mesh and a set of "particles" (water droplets), and that the force applied to the water is only the gravitational force in this phase. The initial position of the water particle inflow, which predicts where the kinetic energy of each particle will initially be lost and gravity will take over, is taken from the results of the Particle Dynamics Simulation (Section 4). We can use the same size particles in this water filling simulation as the particles used in the Particle Dynamics Simulation, or alternately split or merge the particles to adjust for the required precision.

5.1. Pool Segmentation: First, our segmentation method splits the voids of the input into several "pools." We split the pools horizontally (assuming gravity acts vertically) at critical points where the

direction of the water flow changes (Figure 5.1 (a)). We group together pools that will be filled simultaneously when we simulate the water filling state into *filling groups*. We further split pools as new critical points are encountered such that pools in the same filling group have common lower limits and upper limits. This is based on the fact that the water levels of the pools that fill simultaneously are always the same (Section 5.2). A critical point corresponds to a topology change between horizontal slices just below and above the critical point. We can robustly identify all such topology changes using McMains' sweep plane algorithm [18, 19].
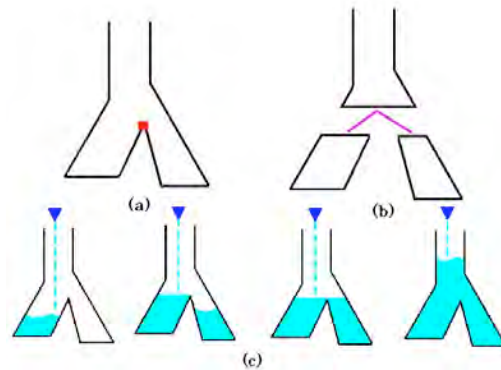

Figure 5.1. (a) The red square shows a critical point at a topology change. (b) Our segmentation method splits a void into different pools when we encounter such topology changes. (c) The segmentation into pools reflects the filling state transitions.

We built a data structure that captures the connectivity of the pools so that we can trace where the water flows and locate where the water can become trapped. If we view these connectivities as a whole, they can be regarded as a tree data structure whose edges correspond to the connectivities and whose nodes correspond to the pools with their associated volumes. Each pool has a fixed volume of water it can hold, except for the pool representing the exterior of the part, which has infinite volume. Figure 5.2 shows the result of our pool segmentation algorithm and the corresponding tree data structure.

5.2. Water Distribution: As described above, we approximate the amount of water with a set of particles that have equal volume. For each particle, we locate the pool where it settles. When the appropriate pool is located, then we add the volume of the particle to that pool. The pools which become full correspond to the parts of the input where the water is trapped.

(a)

(b)

(c)
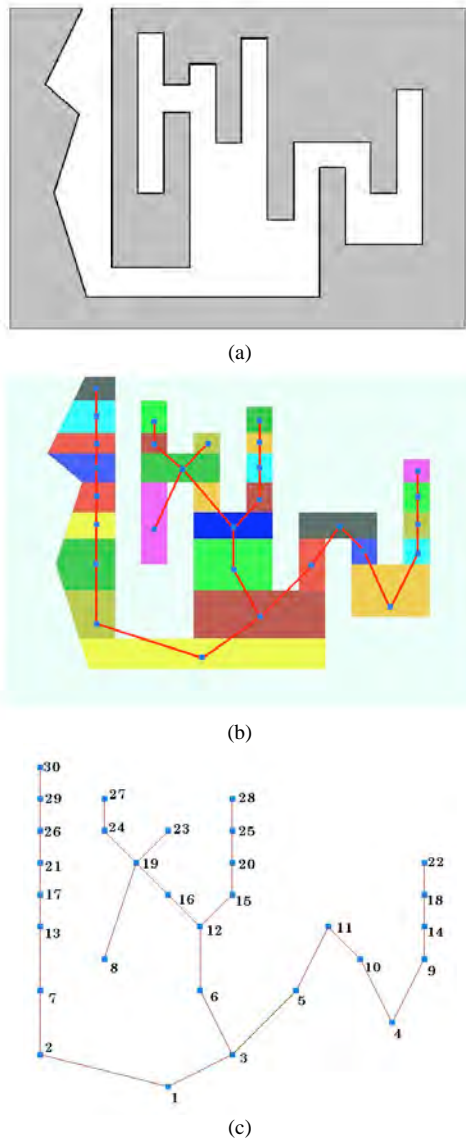
Figure 5.2. (a) Example Input (b) Corresponding segmentation of the void and connectivities of its pools. Different colors indicate different pools. The void is segmented locally at topology changes, and in addition, we split it such that the pools filled simultaneously have the same lower and upper height limit. (c) Corresponding tree structure.

We locate the pool where each particle settles as follows. We assume the node where the particle flows into is given by the Particle Dynamics Simulation. From that node, first, we descend the tree as long as the current node has edges below it. The algorithm to choose which edge to follow at branches is being developed by our industrial partner and is outside the scope of this paper. After locating the appropriate node with no edges below it, we check whether the node is full or not. If it is not full, we add the volume of the particle to the node and go on to the next particle.

If it is already full, we check nodes above this lowest node. If at least one of these nodes above has other non-full nodes below it, we distribute the water to these nodes, descending the tree from there in the same manner recursively. An example of this case can be seen in Figure 5.2 (c) when the water particles flow in from node 30 and nodes 1, 2, 3, 5, 6, and 7 are full. The particle goes up node 11, then descends down node 10, and then 4, instead of up to 12 or 13. If the lowest node has no such nodes above, that is, nodes above that do not have other non-full nodes below, we distribute water upward until we find the node that is not full where the particle settles.

After we find this node, we add the particle volume to the node volume, and based on the tree structure and fill state, possibly modify the tree data structure to combine nodes together in order to speed up the simulation. Figure 5.3 shows some representative states of the tree structure as nodes fill and combine. The transition proceeds from the upper left (initial state) to the lower right. In this model, the lowest node is never deleted and, as a result, nodes extending from the lowest node to the ones above are always nodes currently filled with water. Figure 5.4 shows how the water filling state transitions using our algorithm.
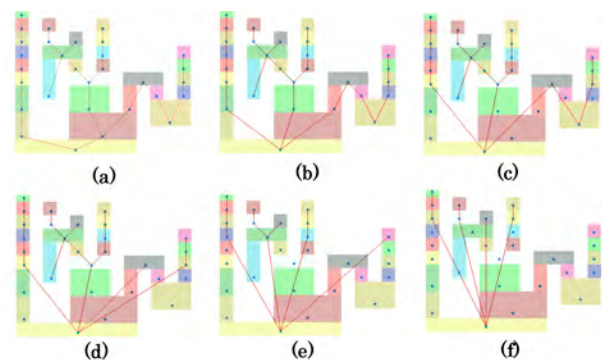
Figure 5.3. Modification of the tree data structure. The transition proceeds from (a) to (f)
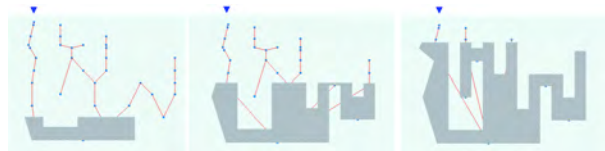
Figure 5.4. Selected transitions of the water filling state. The left corresponds to (a), the center corresponds to (d), and the right corresponds to (f) in Figure 5-3.

6. Summary: Key developments of our work include:

- New measurement methods – the embedded sand method and patterned surface method – that quantify the effect of pressure, angle of attack, standoff distance, and transient loading components including number of impact cycles and waterjet traversal speed on waterjet cleaning effect. Major findings include: cleaning effect does not drop significantly before reaching an attack angle of more than 75°, and an increase in number of loading cycles and frequency from rotating waterjet nozzle carriers significantly improves cleaning effect.

- A macro scale visualization and simulation module that helps in visualizing the interaction of the part geometry with the waterjet. This module can be used to give rough estimates of the variation in cleaning effectiveness due to changes in the cleaning process parameters. We have also used this model to optimize a simplified cleaning process. We found that the results of the optimization agree very closely to the values currently used in industry.

- A particle dynamics module to simulate the local-scale effect of a waterjet striking a surface. This module is used to determine the stress on the surface and the outflow conditions in terms of process and surface parameters. We determined that quantities such as the kinetic energy reach a constant value as the number particles is increased while decreasing their size subject to the constraint that their volume fraction is fixed. This suggests that the waterjet can be modeled with particles that are larger than the real size of the water droplets, leading to a computationally efficient algorithm. Parameter studies were conducted to determine the stresses caused by and the outflow of the waterjet in terms of angle of attack, density of droplets in air, and curvature of the surface.

- A water flow simulation module to predict cleaning-incompatible features of workpieces as an alternative to CFD simulations that would require insurmountable computational expense. We model the flow of water upon waterjet impact as discrete volumes or particles that follow gravity along the maximum gradient of the surfaces. The sequence of cavity filling depends on the connectivity of voids and topological changes along connectivity trees that are identified using our Sweep Plane Algorithm.

8. References:

[1] M. Avila, J. Gardner, C. Reich-Weiser, S. Tripathi, A. Vijayaraghavan, and D. Dornfeld, "Strategies for Burr Formation and Cleanability in Aerospace and Automotive Manufacturing", *SAE J. Aerospace*, 114 (1), pp. 1073-1082, 2005.

[2] M. Avila, C. Reich-Weiser, D. Dornfeld, and S. McMains, "Cleanability Issues in High Performance Cutting*", CIRP Proc. 2nd Intl. Conf. HPC* (CDROM), 2006.

[3] M. Hashish and J.M. Reichman, "Analysis of Waterjet Cutting at High Traverse Rates", *Proc. BHRA 5th Int'l Symposium on Jet Cutting Technology*, paper B2, June 1980.

[4] M. Hashish, M.P. duPlesis, "Theoretical and Experimental Investigation of Continuous Jet Penetration of Solid" *ASME Trans. Engineering for Industry*, Feb. 1978.

[5] F. Erdmann-Jesnitzer, A.M. Hassan and H. Louis, "A Study of the Oscillations Effects on the Cleaning and cutting Efficiency of High Speed Water Jet", *BHRA 3rd Int'l Symposium on Jet Cutting Technology*, Chicago, pp. C3/27-41, 1976

[6] P. Meng, E.S. Geskin, M.C. Leu, and F. Li, "An Analytical and Experimental Study of Cleaning with Moving Waterjets" *ASME Journal of Manufacturing Science and Engineering*, Vol. 120, pp. 580-589, 1998.

[7] M.C. Leu, P. Meng, E.S. Geskin, L. Tismeneskiy, "Mathematical Modeling and Experimental Verification of Stationary Waterjet Cleaning Process," *ASME Journal of Manufacturing Science and Engineering*, Vol. 120, pp. 571-579, 1998.

[8] F. Erdmann-Jesnitzer, H. Louis and J. Wiedemeier "Material Behavior, Material Stressing, Principle Aspects in the Application of High Speed Waterjets", *Proc. BHRA* 4th Int'l Symposium on Jet Cutting Technology, Canterbury, England, pp. E3/29-44, 1978.

[9] M. Vijay, W. Yan, B. Ren, A. Tieu and B. Daniels, "Removal of Hard Metallic and non-Metallic Aerospace Coatings with High-Fequency Forced Pulsed Waterjet Machine",

[10] M. Vijay, "Fluid Mechanics of Jets", Chapter in An Overview of Waterjet Fundamentals and Applications, 5th Edition, Waterjet Technology Association, St Louis, Missouri, pp. w.1/2-28, 2001.

[11] G. Springer, *Erosion By Liquid Impact*, Scripta Publishing, Wiley, pp. 1-123, 1976.

[12] M.C. Rochester, J.H. Brunton, "High Speed Impact of Liquid Jets on Solids", *Proc. BHRA 1st Int'l Symposium on Jet Cutting Technology*, Cranfield, England, pp. A/1-24, 1972.

[13] K. Yanaida and A. Ohashi, "Flow Characteristics of Water Jets in Air", *Proc. BHRA 5th Int'l Symposium of Jet Cutting Technology*, Hannover, Germany, pp. 33-44, 1980.

[14] Matthew Wall, "GAlib: A C++ Library of Genetic Algorithm Components", http://lancet.mit.edu/ga/.

[15] Jasbir S. Arora, Introduction to Optimum Design, Elsevier, pp.558-560, 2004.

[16] Workshop on Cleanability in Manufacturing, http://www.me.berkeley.edu/cleanability/, UC Berkeley, 2007

[17] T.I. Zohdi, "Modeling and Direct Simulation of Near-Field Granular Flows", The International Journal of Solids and Structures, Vol 42/2, pp. 539-564, 2004.

[18] S. McMains and C. Séquin, "A Coherent Sweep Plane Slicer for Layered Manufacturing', *Proc. 5th ACM Symposium on Solid Modeling and Applications*, pp. 285–295, 1999.

[19] S. McMains, "Geometric Algorithms and Data Representation for Solid Freeform Fabrication", PhD Thesis, U.C. Berkeley, 2000.